Electrocatalysis (2021) 12:264–271
https://doi.org/10.1007/s12678-021-00647-w

ORIGINAL RESEARCH

Hydrogen Peroxide Oxidation Reaction on a 4-Mercaptopyridine Self-Assembled Monolayer on Au(111) Metallized by Platinum Nanoislands

Mathias Piescheck[1] · Areeg Abdelrahman[1] · Johannes M. Hermann[1] · Heiko Müller[1] · Timo Jacob[1,2] · Ludwig A. Kibler[1]

Accepted: 1 February 2021 / Published online: 27 February 2021

Abstract
A systematic investigation of the hydrogen peroxide oxidation reaction (HPOR) in phosphate buffer (pH = 7.3) on an Au(111) single crystal modified with a 4-mercaptopyridine self-assembled monolayer (SAM) has been conducted before and after metallization with Pt. While bare Au(111) shows considerable electrocatalytic activity towards the HPOR, the inhibition of the oxidation reaction after modification with the SAM implies that adsorbed 4-mercaptopyridine molecules do not catalyze the HPOR. However, SAM-modified Au(111) recovers catalytic activity for the HPOR already after a single metallization step fabricating Pt islands on-top. Hydrogen peroxide (HP) may then either react at the (non-metallic) Pt nanoislands or on reactivated Au sites, made accessible by structural changes of the SAM induced by the metallization. The shape of the voltammetric profiles for the HPOR on repeatedly metallized SAMs suggests that the contribution of Au to the total current density gradually diminishes with increasing Pt coverage while the contribution of the Pt islands increases. The electrochemical behavior is dominated by the Pt islands at a coverage of 0.5 ML obtained by three subsequent metallization steps.

Keywords Electrocatalysis · Self-assembled monolayers · Metallization of organic layers · Hydrogen peroxide oxidation

Introduction

About one decade ago, Dieter Kolb and co-workers developed an electrochemical enzymatic glucose sensor based on pyranose oxidase immobilized on a Pt-metallized self-assembled monolayer (SAM) on Au(111) [1, 2]. Electrochemically deposited Pt nanoislands of monoatomic height were used as pedestals on which enzyme molecules were wired via poly-allylamine as a linking agent. Only a single enzyme molecule is expected to occupy a Pt island due to its small size in the nanoregime. Taking advantage of the homogeneous distribution of the islands across the SAM, uniform coverage of the enzyme can be achieved. It was assumed that the Pt islands are electrocatalytically active towards the oxidation of hydrogen peroxide (HP) (Fig. 1) generated by pyranose oxidase during the enzymatic glucose oxidation [1, 2]. Amperometric measurements indeed showed a noticeable stepwise increase of the oxidation current after successive addition of glucose rendering the assumption of catalytic activity of the Pt islands towards the HP oxidation reaction (HPOR) plausible since Pt is well-known to be an efficient HPOR catalyst. The processes of the HPOR and the hydrogen peroxide reduction reaction (HPRR) on Pt have extensively been studied during recent decades [3–9]. Due to the good catalytic performance, Pt is commonly used in HP generating enzyme electrodes [10–14]. However, the HPOR itself had not been tested

✉ Ludwig A. Kibler
ludwig.kibler@uni-ulm.de

Mathias Piescheck
mathias.piescheck@uni-ulm.de

Areeg Abdelrahman
areeg.abdelrahman@uni-ulm.de

Johannes M. Hermann
johannes.hermann@uni-ulm.de

Heiko Müller
heiko.mueller84@web.de

Timo Jacob
timo.jacob@uni-ulm.de

[1] Institut für Elektrochemie, Universität Ulm, 89069 Ulm, Germany

[2] Helmholtz-Institut Ulm, 89081 Ulm, Germany

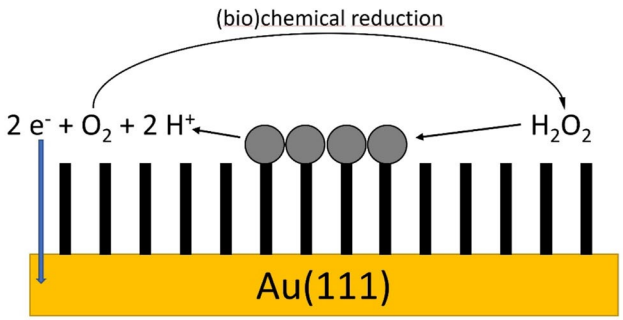

Fig. 1 Model of the platinized SAM utilized by Kolb et al. [2]. The enzyme pyranose oxidase is immobilized on the metallized SAM and converts glucose to glucosone and oxygen to HP. The HP is oxidized electrochemically on the Pt islands to regenerate oxygen while creating an anodic current. The black bars represent 4,4′-dithiodipyridine molecules, gray circles are Pt atoms

explicitly on the Pt islands rendering the reported results only an assumption that HP was oxidized on the islands.

In 2004, Kolb and co-workers provided the first reports of the preparation of metal nanoislands on top of a SAM [15]. A method was introduced to deposit Pd islands of monoatomic height and few nanometers in diameter on a 4-mercaptopyridine SAM on Au(111) (made from 4,4′-dithiodipyridine) by electroless adsorption of Pd^{2+} ions from a $PdSO_4$ solution presumably on the pyridinic nitrogen followed by an electrochemical reduction of the adsorbed Pd^{2+} ions in a solution freed from metal ions. Later on, the same procedure was successfully applied to metallize the SAM with Pt and Rh islands [16, 17]. Until recently, various, similar approaches of SAM metallization were developed [18–20]. The key point of those metallization procedures is the presence of heteroatoms in the SAM molecules that are capable of coordinating and capturing metal ions. The use of well-ordered single crystal substrates is important since defects may allow the metal ions to penetrate the SAM and deposit directly on the substrate.

Recently, the catalytic activity and various structural and electrochemical properties of Pt and Pd nanoislands towards the oxidation of carbon monoxide and methanol have been studied [21]. The metal islands show some catalytic activity towards these reactions although they are non-metallic. The electrocatalytic activity increases with Pt or Pd coverage while the SAM-covered Au (111) is inactive.

In this work, a systematic investigation of the HPOR on the hierarchical Au(111)-SAM-Pt system without enzymes is presented and the question of whether the Pt islands show catalytic activity for the hydrogen peroxide oxidation reaction is addressed. For that purpose, the properties of Au(111), of SAM-modified Au(111), and the Pt metallized SAM on Au(111) have been studied before and after adding HP.

Experimental

The preparation of the Pt-metallized SAM was carried out following Kolb's method with slight modifications [15]. The Au(111) crystal (MaTecK, Jülich, Germany, 4 mm diameter, 0.126 cm^2 surface area) was flame-annealed before dipping for 10 min into a deaerated 20 µM solution of 4,4′-dithiodipyridine (Acros, 98%) in ultrapure water (18.2 MΩ cm, < 5 pbb TOC). During the adsorption process, the S–S bond of 4,4′-dithiodipyridine breaks to form two molecules of 4-mercaptopyridine adsorbing on the Au surface via the S atom. The modified crystal was then rinsed with ultrapure water and dipped into a solution of 0.1 mM $K_2[PtCl_4]$ (Aldrich, 99.99%) in 0.1 M H_2SO_4 for 2 min without potential control. The crystal was again rinsed with water and transferred to an electrochemical cell filled with 0.1 M H_2SO_4. The metal species complexed by pyridinic nitrogen of the SAM were reduced electrochemically during a linear sweep from 0.5 to − 0.2 V *vs*. SCE at a scan rate of 5 mV s^{-1}. For subsequent metallization steps, the complexation in the metal ion containing solution and the electrochemical reduction were repeated in the same manner. After the metallization, the crystal was rinsed with water and transferred to an electrochemical cell containing 50 mL of a phosphate buffer solution (PBS, 0.1 M total phosphate content). The phosphates used were NaH_2PO_4, Na_2HPO_4 (VWR, AnalaR NORMAPUR), and KH_2PO_4, K_2HPO_4 (Merck, EMSURE). After the measurements with the pure buffer solution, 50 µL of a 1 M HP solution (Merck, 30%) was added via an Eppendorf pipette. The counter electrode was a Pt wire and a saturated calomel electrode (SCE) was used as reference electrode. For comparative measurements of the HPOR on bulk Pt, a flame-annealed polycrystalline Pt wire was used as a working electrode. The electrochemically active surface area (0.334 cm^2) was determined by the hydrogen adsorption method (210 µC cm^{-2} total charge density) using the voltammogram shown in Fig. 4c inset (brown curve) [22, 23]. All potentials reported in the text are quoted versus the SCE reference. For the sake of comparison, a potential axis referenced versus the reversible hydrogen electrode (RHE) is included in all figures. All media used for electrochemistry were purged with nitrogen before and during the measurements to remove molecular oxygen.

Results and Discussion

HPOR on a Bare Au(111) Surface

The HPOR was investigated systematically, starting with the unmodified Au(111) surface in contact with the phosphate buffer solution at pH 7.3 (Fig. 2). In the absence

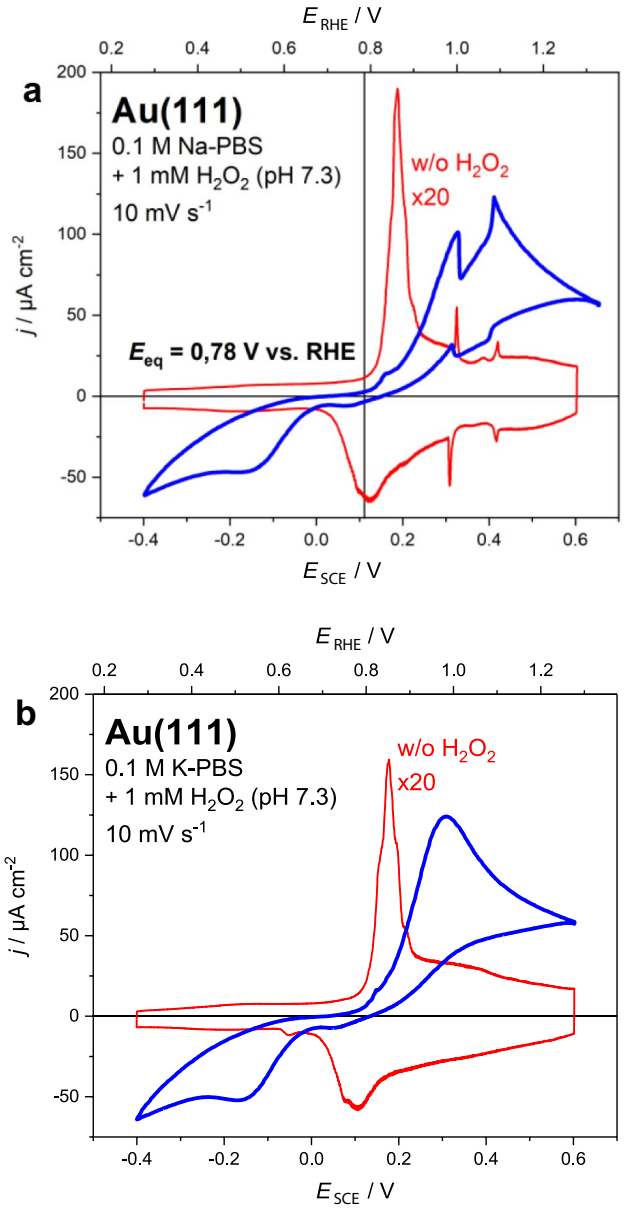

Fig. 2 **a** Cyclic voltammogram of Au(111) in 0.1 M Na-PBS pH 7.3 (red) and HPOR/HPRR after addition of 1 mM H_2O_2 (blue). The black vertical line marks the equilibrium potential of the HPOR [29]. **b** Cyclic voltammogram of Au(111) in 0.1 M K-PBS pH 7.3 (red) and HPOR/HPRR after addition of 1 mM H_2O_2 (blue). Scan rate: 10 mV s^{-1}

of HP (red curves), the lifting of the surface reconstruction by specific adsorption of phosphate is observable at 0.19 V [24]. The structure of the phosphate adlayer is strongly influenced by co-adsorption of cations. This is obvious from phase transitions in the presence of sodium ions (Fig. 2a) [25], which are absent for the phosphate buffer solution with potassium ions (Fig. 2b). The HPOR starts close to the equilibrium potential of HPOR (0.78 V *vs*. RHE and 0.11 V *vs*. SCE for pH 7.3 and 1 mM HP, vertical line in Fig. 2a). Obviously, the HPOR takes place on the unreconstructed surface and the presence of the ordered Na phosphate adlayer slightly diminishes the catalytic activity in the potential region between the sharp current spikes (Fig. 2a). For comparison, the same experiment was done for Au(111) in a potassium phosphate buffer solution (Fig. 2b, red curve) and no spikes could be observed which is in accordance with the literature [24, 26]. The Na phosphate adlayer diminishes the current density by about 20–30%. In the presence of either Na^+ and K^+ ions, the voltammetric response of the HPOR shows a decrease in current density at positive potentials, which is typically attributed to diffusion limitation [27]. During phosphate adsorption, water molecules are partially discharged to form adsorbed OH [27, 28], which is supposed to react chemically with HP (Fig. 2a, b, blue curves) forming a reduced Au surface as well as H_2O and O_2 according to Eq. (1) [27]. The measured anodic current is caused by the re-oxidation of the Au surface, as shown in Eq. (2).

$$2\,\mathrm{Au(OH)} + \mathrm{H_2O_2} \rightarrow 2\,\mathrm{Au} + 2\mathrm{H_2O} + \mathrm{O_2} \quad (1)$$

$$2\,\mathrm{Au} + 2\mathrm{H_2O} \rightarrow 2\,\mathrm{Au(OH)} + 2\mathrm{H^+} + 2\mathrm{e^-} \quad (2)$$

Voltammetric studies imply that the electrochemical step (Eq. (2)) is slower than the purely chemical reaction (Eq. (1)) [27] rendering the overall reaction rate potential dependent at lower overpotentials. The increasing reaction rate due to increasing anodic potential leads to a rapid conversion of HP causing a high peak current. Indeed, surface enhanced Raman spectroscopy (SERS) measurements show that adding HP to the electrolyte completely erases the OH_{ad} vibration band up to a potential of approximately 0.35 V [30] giving experimental evidence that the electrochemical surface oxidation is slower than the chemical surface reduction performed by HP. However, above 0.35 V, the OH_{ad} vibration band slowly reappears indicating that the electrochemical OH formation is no longer slower than the chemical reaction. RDE studies show a steady decrease in the overall reaction rate [27] explaining the anodic current decrease above 0.35 V. This decrease does not seem to be caused by an "ordinary" diffusion limitation due to rapid HP depletion. It has been supposed that the increasing amount of adsorbed species (OH, anions) or a changing water structure close to the electrode surface strongly hinder the diffusion of HP to the electrode and therefore, drastically lower the reaction rate [27]. Consequently, the measurable peak current density should be lower than in the case of a purely diffusion-driven process. A theoretical peak current of a diffusion-controlled HP oxidation can be determined from the Randles-Ševčík equation. Assuming a diffusion coefficient for HP of 0.66×10^{-5} cm^2 s^{-1} [3], a peak current

density of about 200 µA cm^{-2} can be estimated at 25 °C and a scan rate of 10 mV s^{-1}. This value is noticeably larger than the peak current density of approximately 125 µA cm^{-2} shown in Fig. 2a, b.

In the pH range around 7, the strongly adsorbing PO_4 species is predominant on the Au surface [31]. This species can adsorb triply coordinated via three free oxygen atoms on the hexagonal Au surface lattice. Recent studies identified HPO_4 and PO_4 as site blocking species during the electro-oxidation of formic acid (FAOR) [32]. While PO_4 blocks FAOR almost completely, its effect on the HPOR is less pronounced. In general, as a result of the competitive nature of anion adsorption, the overall HPOR current on Au(111) in PBS seems to be smaller than in electrolytes with weakly adsorbing anions, such as ClO_4^- [27].

The HPRR along with the reduction of O_2 generated during the HPOR occurs below 0 V and proceeds similarly in both Na-PBS and K-PBS due to the absence of phosphate adsorption in this potential range and a negligible effect of the cation.

HPOR on the SAM-Modified Au (111) Surface

The 4-mercaptopyridine SAM causes significant changes in the voltammetric behavior (Fig. 3, red curve) and masks characteristic features of the bare Au(111) (compare Fig. 2), e.g., the lifting of the surface reconstruction and the sodium ion induced phase transitions of the phosphate adsorption layer. The potential window in Fig. 3 marks the stability region of the SAM. The lower boundary is set by the reductive desorption of the SAM, whereas the higher boundary is limited by the Au surface oxidation starting at ca. 0.65 V under these experimental conditions. Above 0.3 V, a slight current increase and a corresponding broad counter peak can be noticed (Fig. 3). After the addition of HP, a small but rather noticeable oxidation current occurs (Fig. 3, blue curve). This oxidation current might correspond to the HPOR at defect sites on the underlying Au surface or an HP-assisted decomposition of the SAM. However, compared with the oxidation current on bare Au shown in Fig. 2, the current is 50-fold smaller and thus not significant.

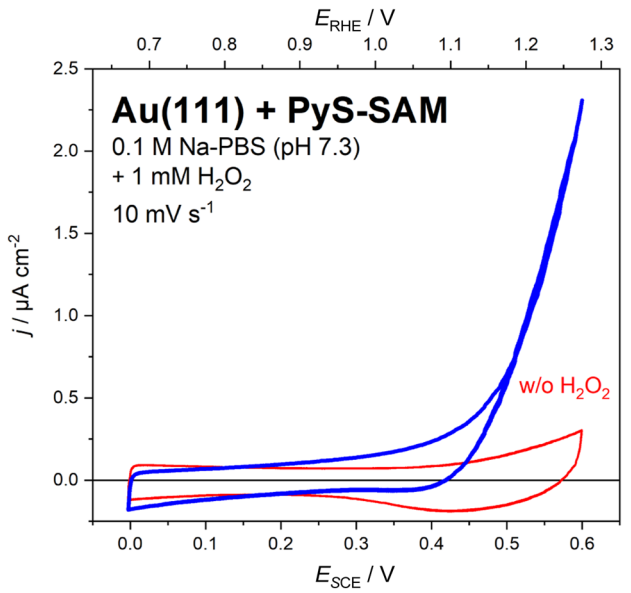

Fig. 3 Cyclic voltammograms for Au(111) modified with 4-mercaptopyridine (PyS) in 0.1 M Na-PBS pH 7.3 (red) and after addition of 1 mM H_2O_2 (blue). Scan rate: 10 mV s^{-1}

Obviously, the 4-mercaptopyridine SAM itself does not show a substantial catalytic activity towards the HPOR. In-situ scanning tunneling microscopy (STM) studies reveal that the 4-mercaptopyridine SAM mostly shows a $\left(7 \times \sqrt{3}\right)$ and $\left(5 \times \sqrt{3}\right)$ superstructure of π-stacked stripes on Au(111) [33], whereas DFT calculations confirmed that the $\left(7 \times \sqrt{3}\right)$ structure is the thermodynamically more stable one [34]. The theoretical calculations also showed that in both cases, the SAM molecules preferably adsorb at Au bridge sites which is also the preferred adsorption site of OH [35, 36]. Moreover, due to the tilt of the 4-mercaptopyridine molecules, adjacent adsorption sites are sterically blocked [34]. Both the direct occupation and the steric shielding of the favored OH adsorption sites explain the strong inhibition of the HPOR at a SAM coverage of about 20% under these experimental conditions ($\theta = 3/14$ and $\theta = 1/5$ ML for the $\left(7 \times \sqrt{3}\right)$ and the $\left(5 \times \sqrt{3}\right)$ superstructure, respectively) [21, 33, 34].

HPOR on the Pt-Metallized SAM on Au(111)

Pt metallization leads to a significantly higher activity towards the HPOR compared with the non-metallized SAM (Fig. 4a, red curve *vs*. Fig. 3, blue curve). Interestingly, the shape of the oxidation curve for HPOR with Pt nanoparticles deposited onto the SAM is very similar to that obtained for unmodified Au(111) (Fig. 4a, red *vs*. green curve). The occurrence of a pronounced oxidation peak followed by a decrease in current is a typical feature of HPOR on Au (see Fig. 3, [27]). Contrarily, this voltammetric feature is clearly different for the HPOR on polycrystalline Pt as it shows a current plateau (Fig. 4c). It can clearly be stated that hydrogen peroxide is oxidized after metallizing the 4-mercaptopyridine SAM on Au(111) with Pt nanoislands, which answers the main question of this study. However, both Au and Pt sites have to be taken into account regarding the active centers of HPOR. While the Pt nanoislands are located on-top, their metallic properties are not fully developed after a single metallization step

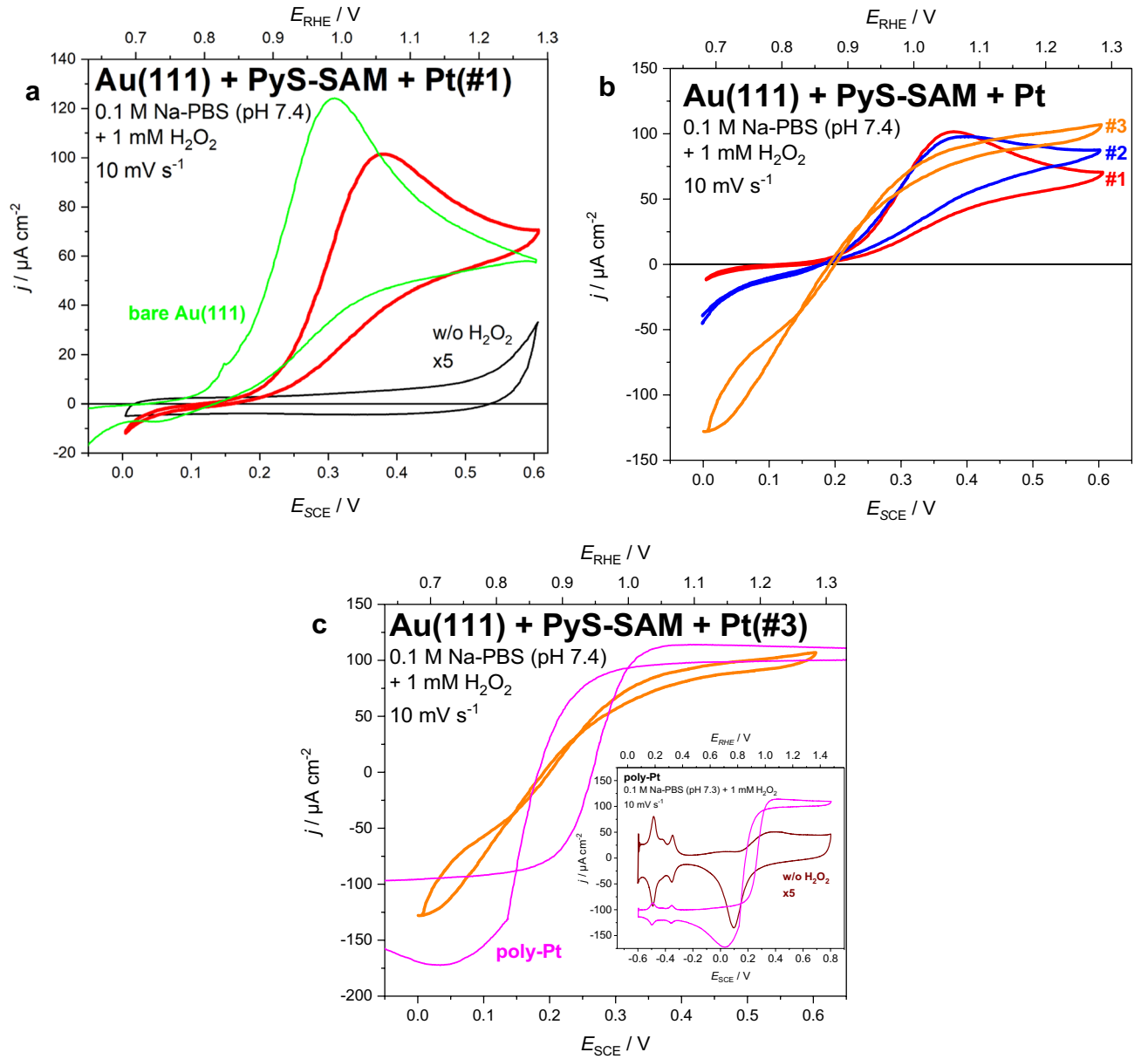

Fig. 4 **a** Cyclic voltammogram of singly metallized (Pt#1) SAM on Au(111) in 0.1 M Na-PBS pH 7.3 before (black) and after addition of 1 mM H_2O_2 (red). The green curve shows the HPOR on bare Au(111) in 0.1 M K-PBS for the sake of comparison. **b** HPOR on multi metallized SAM on Au(111) including the different metal coverages for the first (#1, red), second (#2, blue), and third metallization (#3, orange). **c** HPOR on a triply metallized SAM (orange) and poly-Pt (magenta). The inset shows cyclic voltammograms for poly-Pt in 0.1 M Na-PBS pH 7.3 before (brown) and after the addition of 1 mM H_2O_2 (magenta). Scan rate: 10 mV s^{-1}. Curves with the same color are identical

(see Fig. 4). In addition, as noted above, the voltammetric signal, i.e., the peak shape is very much Au-like, while the SAM itself shows almost no HPOR activity prior to metallization. Indeed, in situ STM studies reveal structural changes of the SAM after metal deposition [15, 16, 21]. The molecules of a well-ordered unmetallized SAM show a mostly uniform orientation of the pyridine ring, which leads to almost complete blocking of the Au surface for HPOR (blue curve in Fig. 3). The metallization with Pt causes a restructuring of the adsorbed 4-mercaptopyridine molecules, which might lead to a partial reactivation of the underlying Au(111) surface. Obviously, the SAM structure can differ below and in the neighborhood of the Pt islands. Furthermore, due to the strong affinity between Pt atoms and the pyridinic nitrogen, Pt islands may tighten adjacent SAM molecules. Characteristics of Au gradually disappear for repeated platinization, while the behavior gets more and more Pt-like (see Fig. 4).

Besides the reactivation of the Au substrate for HPOR, the Pt islands seem also to contribute to the overall electrocatalytic activity. It is known that metal nanoparticles on top of an SAM can restore the electron transfer through the adsorbed molecules to the underlying electrode [37, 38]. In the presence of metal nanoparticles, electrons can hop to the Au(111) surface and vice versa. It is supposed that the adsorption capability increases with increasing Pt coverage, which is a prerequisite of catalyzing a Faraday reaction, i.e., electrocatalysis.

The question of whether Au or the Pt islands provide the active sites for the HPOR has not been addressed by Kolb and co-workers [1, 2]. A single metallization step was used and it was assumed that the Pt islands are catalytically active. The present results indicate that also Au contributes to the overall activity. Repeated metallization changes the shape of the oxidation curve gradually towards the behavior of bulk Pt (Fig. 4b, c). This behavior indicates an increasing influence of Pt on the HPOR. The voltammogram of the triply metallized SAM clearly shows typical Pt features. These include (i) no rapid current decay at positive potentials, (ii) a loop between 0.15 and 0.3 V corresponding to the hysteresis of the OH adsorption and desorption, and (iii) the similar activity of the HPRR and the reduction of O_2 generated during the HPOR determined for a quiescent electrolyte. The Pt coverage on the SAM is determined by the charge density for electrodeposition of the adsorbed metal ions (not shown). Considering a charge density of 444 μC cm^{-2} for a complete monolayer [39], the first, second, and third metallization steps yield coverages of 0.17, 0.33, and 0.49, respectively, which is in accordance with previous studies [21].

The HPOR occurs in a potential region where OH adsorption takes place on Pt (inset of Fig. 4c). Recent infrared studies confirm the existence of adsorbed OH in the potential region above 0.8 V *vs*. RHE [40]. Analogous to Au, the HPOR on Pt is usually described as follows [3, 29]:

$$Pt(OH)_2 + H_2O_2 \rightarrow Pt + 2H_2O + O_2 \quad (3)$$

$$Pt + 2H_2O \rightarrow Pt(OH)_2 + 2H^+ + 2e^- \quad (4)$$

HP reacts with adsorbed OH to form molecular oxygen and free Pt sites (Eq. (3)), which are reoxidized electrochemically (Eq. (4)) generating an anodic current. In the case of Pt, RDE studies show that the electrochemical re-oxidation of the Pt surface is faster than the chemical surface reduction [3, 4]. At sufficiently high overpotentials, there is always enough $Pt(OH)_2$ that can react chemically with HP. Hence, the chemical reaction is rate-limiting. This would explain the apparent potential independence of the anodic current above 0.35 V (Fig. 4c). Extensive studies of the HPOR on Pt revealed an adsorption-controlled reaction mechanism with Michaelis–Menten-like kinetics (Eq. (5)) [3]:

$$Pt(OH)_2 + H_2O_2 \rightleftharpoons Pt(OH)_2 \bullet H_2O_2 \rightarrow Pt + 2H_2O + O_2 \quad (5)$$

Equation (5) is an extension of Eq. (3). $Pt(OH)_2$ acts as a binding site on which HP can adsorb reversibly [3].

Calculations have shown that the fractional surface coverage should remain constant at sufficiently high overpotentials [4]. The adsorption is then followed by an internal charge transfer. The above description does not include inhibition effects. In fact, two reaction products, O_2 and H^+, which are formed during the chemical and the electrochemical reaction, respectively, competitively adsorb on the $Pt(OH)_2$ binding sites. The steady-state rate of product formation is given by inhibited Michaelis–Menten kinetics [3].

The reaction rate decreases with increasing O_2 and H^+ concentrations. This explains the almost linear anodic current decrease observed for Pt above 0.35 V, which continues in the negative scan as more reaction products have been accumulated (Fig. 4c inset). In general, the steady-state current above 0.35 V is higher than the current observed on Au. Pt does not seem to exhibit such a strong inhibition of the HPOR at high overpotentials rendering Pt a better catalyst for the HPOR at more anodic potentials.

However, neither phosphate nor direct OH adsorption has been observed on the Pt nanoislands on the SAM (Fig. 4a, black curve). Then again, the HPOR still occurs in the same potential range where the partial discharge of the hydration shell of adsorbed phosphate on Au and direct OH adsorption on Pt takes place. The voltammetric measurements imply that the HPOR on the metallized SAM is a hybrid case between Au and Pt. Since the HPOR mechanisms on bare Au and Pt involve adsorbed OH, the reaction mechanism on metallized SAMs should still involve adsorbed OH although the OH adsorption cannot be observed directly. Nonetheless, details of the reaction mechanism remain unknown and the catalytic activity of Pt metallized SAMs cannot be described in more detail within the scope of the present study.

While a Pd monolayer with metallic properties can be obtained after two metallization steps (70% coverage), Pt does not show metallic behavior [41]. Although ultraviolet photoelectron spectroscopy (UPS) measurements for a Pt monolayer with 50% coverage show an insulator-like character, the presented electrochemical measurements clearly exhibit a behavior for HPOR close to metallic Pt (Fig. 4c) [21]. Therefore, full metallicity does not seem to be a requirement for catalytic activity towards the HPOR. However, it is known that already a second atomic layer is partially formed after the third metallization step [21]. This can lead to a few adsorption sites with a behavior close to bulk Pt electrodes, which could explain the observed electrochemical behavior.

Conclusions

In this work, an Au(111) crystal was modified with a 4,4′-dithiodipyridine SAM which was metallized with Pt islands of monoatomic height. The HPOR was investigated on each layer of this hierarchical system. On a bare Au(111) surface, phosphate adsorption shows a strong interference with the HPOR. The presence of sodium ions and the resulting phase transitions of adsorbed phosphate cause significant drops in activity.

SAM-modified Au(111) shows a very low catalytic activity as the SAM effectively prevents OH adsorption which is a crucial requirement for the HPOR.

On a singly metallized SAM, a significant reactivation of the HPOR is observed. However, it is arguable if the reaction takes place exclusively on the Pt islands. Considering the shape of the oxidation wave, which is comparable with the one obtained on Au, a considerable contribution of the underlying Au surface is assumed. The metallization of the SAM leads to structural changes of the SAM, which may expose free adsorption sites for OH on the Au surface. OH adsorption could not be observed directly by voltammetry. However, the HPOR still occurs in the potential range where OH adsorption normally takes place on Au and Pt. Multiple metallization steps cause the voltammogram of the HPOR to shift from an Au-like towards a Pt-like behavior indicating an increasing influence of the Pt islands on the reaction. The voltammetric response on the triply metallized SAM shares some typical features of the one obtained on metallic Pt, although the Pt islands are non-metallic.

Kolb and co-workers used a singly metallized SAM for their enzyme setup. But the question of whether the HPOR takes place on the Pt islands or on the Au surface had not been addressed. Especially in the case of the singly metallized SAM, the assumption of an exclusively Pt island catalyzed HPOR seems debatable. The present investigation shows that a singly metallized SAM on Au does exhibit the ability to oxidize HP and the application of Pt islands in HP generating enzyme setup seems to be justified. Future works will attempt to provide further insights into the HPOR on Pt-metallized SAMs and attempt to answer the question to which extent Au, Pt, or a combination of both delivers the active sites for the HPOR.

Acknowledgements Support by the Fonds der Chemischen Industrie is greatly acknowledged.

Author Contribution Conceptualization: L.A.K.; methodology: L.A.K., M.P., J.M.H.; validation: L.A.K., J.M.H.; formal analysis: M.P.; investigation: M.P., resources: T.J.; data curation: M.P.; writing—original Draft: M.P.; writing—review & editing: L.A.K., J.M.H., A.A., H.M., T.J.; visualization: M.P.; supervision: L.A.K.; project administration: L.A.K.; funding acquisition: T.J.

Funding Open Access funding enabled and organized by Projekt DEAL.

Data Availability All data will be handed out, if requested.

Declarations

Conflict of Interest The authors declare that they have no conflict of interest.

References

1. J. Gajdzik, J. Lenz, H. Natter, R. Hempelmann, G.-W. Kohring, F. Giffhorn, M. Manolova, D.M. Kolb, Enzyme immobilisation on self-organised nanopatterned electrode surfaces. Phys. Chem. Chem. Phys. **12**, 12604 (2010)
2. J. Lenz, J. Gajdzik, H. Natter, R. Hempelmann, G.-W. Kohring, F. Giffhorn, M. Manolova, D.M. Kolb, Platinum islands on SAMs as template for enzyme-catalyzed glucose oxidation. ECS Trans. **33**, 35 (2011)
3. S.B. Hall, E.A. Khudaish, A.B. Hart, Electrochemical oxidation of hydrogen peroxide at platinum electrodes. Part 1: an adsorption-controlled mechanism. Electrochim. Acta **43**, 579 (1998)
4. S.B. Hall, E.A. Khudaish, A.B. Hart, Electrochemical oxidation of hydrogen peroxide at platinum electrodes. Part II: effect of potential. Electrochim. Acta **43**, 2015 (1998)
5. S.B. Hall, E.A. Khudaish, A.B. Hart, Electrochemical oxidation of hydrogen peroxide at platinum electrodes. Part III: effect of temperature. Electrochim. Acta **44**, 2455 (1999)
6. S.B. Hall, E.A. Khudaish, A.B. Hart, Electrochemical oxidation of hydrogen peroxide at platinum electrodes. Part IV: phosphate buffer dependence. Electrochim. Acta **44**, 4573 (1999)
7. S.B. Hall, E.A. Khudaish, A.B. Hart, Electrochemical oxidation of hydrogen peroxide at platinum electrodes. Part V: inhibition by chloride. Electrochim. Acta **45**, 3573 (2000)
8. Y. Zheng, W. Chen, X.-Q. Zuo, J. Cai, Y.-X. Chen, The kinetics of the oxidation and reduction of H_2O_2 at a Pt electrode: a differential electrochemical mass spectrometric study. Electrochem. Commun. **73**, 38 (2016)
9. A. Hickling, W.H. Wilson, The anodic decomposition of hydrogen peroxide. J. Electrochem. Soc. **98**, 425 (1951)
10. I.A. Silver, M. Erecinska, Extracellular glucose concentration in mammalin brain: continuous monitoring of changes during increased neuronal activity and upon limitation in oxygen supply in normo-, hypo-, and hyperglycemic animals. J. Neurosci. **14**, 5068 (1994)
11. L.I. Netchiporouk, N.F. Shram, N. Jaffrezic-Renault, C. Martelet, R. Cespuglio, In Vivo Brain Glucose Measurements: Differential

Normal Pulse Voltammetry with Enzyme-Modified Carbon Fiber Microelectrodes. Anal. Chem **68**, 4358 (1996)
12. M. Ciobanu, D.E. Taylor, J.P. Wilburn, D.E. Cliffel, Glucose and lactate biosensors for scanning electrochemical microscopy imaging of single live cells. Anal. Chem. **80**, 2717 (2008)
13. G.G. Guilbault, G.J. Lubrano, An enzyme electrode for the amperometric determination of glucose. Anal. Chim. Acta **64**, 439 (1973)
14. C. Luhana, X.-J. Bo, J. Ju, L.-P. Guo, A novel enzymatic glucose sensor based on Pt nanoparticles-decorated hollow carbon spheres-modified glassy carbon electrode. J. Nanopart. Res. **14**, 1919 (2012)
15. T. Baunach, V. Ivanova, D.M. Kolb, H.-G. Boyen, P. Ziemann, M. Büttner, P. Oelhafen, A new approach to the electrochemical metallization of organic monolayers: palladium deposition onto a 4,4′-dithiodipyridine self-assembled monolayer. Adv. Mater. **16**, 2024 (2004)
16. V. Ivanova, M. Manolova, D.M. Kolb, Palladium and platinum deposition onto 4-mercaptopyridine SAMs. Solid State Phenom. **121–123**, 363 (2007)
17. M. Manolova, M. Kayser, D.M. Kolb, H.-G. Boyen, P. Ziemann, D. Mayer, A. Wirth, Rhodium deposition onto a 4-mercaptopyridine SAM on Au(111). Electrochim. Acta **52**, 2740 (2007)
18. F. Chesneau, M. Zharnikov, Palladium chloride as seeding and surfactant layer to mediate the formation of top metal films on self-assembled monolayers. J. Phys. Chem. C **118**, 12980 (2014)
19. A. Venäläinen, K. Meinander, M. Räisänen, V. Tuboltsev, J. Räisänen, Metallization of self-assembled organic monolayer surfaces by Pd nanocluster deposition. Surf. Sci. **677**, 68 (2018)
20. Z. She, Z. Yao, H. Ménard, S. Tobish, D. Lahaye, N.R. Champness, M. Buck, Coordination controlled electrodeposition and patterning of layers of palladium/copper nanoparticles on top of a self-assembled monolayer. Nanoscale **11**, 13773 (2019)
21. H. Müller, M. Metzler, N. Barth, B. Conings, H.-G. Boyen, T. Jacob, L.A. Kibler, Electrocatalytic behavior of Pd and Pt nanoislands deposited onto 4,4′-dithiodipyridine SAMs on Au(111). Electrocatalysis **9**, 505 (2018)
22. R. Woods, Hydrogen adsorption on platinum, iridium and rhodium electrodes at reduced temperatures and the determination of real surface area. Electroanal. Chem. and Interfacial Electrochem. **49**, 217 (1974)
23. C.L. Scortichini, C.N. Reilley, Surface characterization of Pt electrodes using underpotential deposition of H and Cu. J. Catal. **79**, 138 (1983)
24. A. Cuesta, M. Kleinert, D.M. Kolb, The adsorption of sulfate and phosphate on Au(111) and Au(100) electrodes: an in situ STM study. Phys. Chem. Chem. Phys. **2**, 5684 (2000)
25. F. Silva, M.J. Sottomayor, A. Martins, A voltammetric study of a surface phase transformation of adsorbed HPO_4^{2-} anion on Au(111) in the presence of Na^+ cations. J. Electroanal. Chem. **375**, 395 (1994)
26. C. Schlaup, S. Horch, In-situ STM study of phosphate adsorption on Cu(111), Au(111) and Cu/Au(111) electrodes. Surf. Sci. **608**, 44 (2013)
27. A.M. Gómez-Marín, A. Boronat, J.M. Feliu, Electrocatalytic oxidation and reduction of H_2O_2 on Au single crystals. Russ. J. Electrochem. **53**, 1029 (2017)
28. H. Angerstein-Kozlowska, B.E. Conway, A. Hamelin, L. Stoicoviciu, Elementary Steps of Electrochemical Oxidation of Single-Crystal Planes of Au - I. Chemical Basis of Processes Involving Geometry of Anions and the Electrode Surface. Electrochim. Acta **31**, 1051 (1986)
29. I. Katsounaros, W.B. Schneider, J.C. Meier, U. Benedikt, P. Ulrich Biedermann, A.A. Auer, K.J.J. Mayrhofer, Hydrogen peroxide electrochemistry on platinum: towards understanding the oxygen reduction reaction mechanism. Phys. Chem. Chem. Phys. **14**, 7384 (2012)
30. X. Li, A.A. Gewirth, Peroxide electroreduction on bi-modified Au surfaces: vibrational spectroscopy and density functional calculations. J. Am. Chem. Soc. **125**, 7086 (2003)
31. M. Yaguchi, T. Uchida, K. Motobayashi, M. Osawa, Speciation of adsorbed phosphate at gold electrodes: a combined surface-enhanced infrared absorption spectroscopy and DFT study. J. Phys. Chem. Lett. **7**, 3097 (2016)
32. A. Abdelrahman, J.M. Hermann, L.A. Kibler, Electrocatalytic oxidation of formate and formic acid on platinum and gold: study of pH dependence with phosphate buffers. Electrocatalysis **8**, 509 (2017)
33. Weiping Zhou, T. Baunach, V. Ivanova, D.M. Kolb, Structure and Electrochemistry of 4,4‘-Dithiodipyridine Self-Assembled Monolayers in Comparison with 4-Mercaptopyridine Self-Assembled Monolayers on Au(111), Langmuir **20**, 4590 (2004)
34. J. Kucera, A. Groß, Adsorption of 4-mercaptopyridine on Au(111): a periodic DFT study. Langmuir **24**, 13985 (2008)
35. A.A. Koverga, S. Frank, M.T.M. Koper, Density functional theory study of electric field effects on CO and OH adsorption and co-adsorption on gold surfaces. Electrochim. Acta **101**, 244 (2013)
36. A.M. Pessoa, J.L.C. Fajín, J.R.B. Gomes, M. Natália, D.S. Cordeiro, Cluster and periodic DFT calculations of adsorption of hydroxyl on the Au(hkl) surfaces. J. Mol. Struc. Theochem **946**, 43 (2010)
37. P. Cea, S. Martín, A. González-Orive, H.M. Osorio, P. Quintín, L. Herrer, Nanofabrication and electrochemical characterization of self-assembled monolayers sandwiched between metal nanoparticles and electrode surfaces. J. Chem. Educ. **93**, 1441 (2016)
38. D. Bethell, M. Brust, D.J. Schiffrin, C. Kiely, From monolayers to nanostructured materials: an organic chemist’s view of self-assembly. J. Electroanal. Chem. **409**, 137 (1996)
39. V. Ivanova, T. Baunach, D.M. Kolb, Metal deposition onto a thiol-covered gold surface: a new approach. Electrochim. Acta **50**, 4283 (2005)
40. H. Tanaka, S. Sugawara, K. Shinohara, T. Ueno, S. Suzuki, N. Hoshi, M. Nakamura, Infrared reflection absorption spectroscopy of OH adsorption on the low index planes of Pt. Electrocatalysis **6**, 295 (2015)
41. H.-G. Boyen, P. Ziemann, U. Wiedwald, V. Ivanova, D.M. Kolb, S. Sakong, A. Gross, A. Romanyuk, M. Büttner, P. Oelhafen, Local density of states effects at the metal-molecule interfaces in a molecular device. Nat. Mater. **5**, 394 (2006)